J. Fluid Mech. (1978), *vol.* 86, *part* 2, *pp.* 293–311
Printed in Great Britain

The entrainment interface in a stratified fluid

By L. R. WYATT

Department of Earth and Planetary Sciences, The Johns Hopkins University, Baltimore, Maryland 21218

(Received 3 March 1977 and in revised form 14 November 1977)

A study is made of the entrainment interface in a two-layer flow with one layer turbulent owing to an imposed surface stress. Turbulent and wave parameters were measured from films of an experiment carried out by Kantha, Phillips & Azad (1977) and are analysed to determine relationships between wave and turbulent length and velocity scales and bulk scales.

A measure of interface distortion is calculated and it is found to be related to the mixed-layer depth only at small overall Richardson number. The local velocity of advance of the interface is determined and is found to vary with overall Richardson number tending to the Kolmogorov scale at small Ri and to Phillips' (1966) quasi-laminar scale at large Ri.

Kelvin–Helmholtz type instabilities are observed and their wavelength, amplitude and lifetime are measured. The wavelength is not found to be related to the mixed-layer depth but some dependence on overall Richardson number is observed. An interfacial mean flow Richardson number is estimated and the variation of wave slope at maximum amplitude with this Richardson number is found to be comparable with observations of Thorpe (1973*a*) in a laminar two-layer flow. A relationship between the wavelength of an instability and the distortion length scale is found and is discussed.

1. Introduction

The study of entrainment in stratified fluids has been restricted mainly to the determination of an averaged entrainment rate in terms of overall length, velocity and density scales of the flow usually expressed in the form of a Richardson number. Laboratory experiments (Turner 1968; Kato & Phillips 1969; Moore & Long 1971) have shown that power law relationships between entrainment rate and Richardson number agree well with data. Kantha *et al.* (1977) found a more general entrainment rate to Richardson number relationship, although this could be approximated by a series of power laws over limited ranges of Ri. Studies of entrainment at the base of the oceanic mixed layer (Kraus & Turner 1967; Denman 1973; Turner 1969) have used parameterizations which are essentially power laws of this type. An alternative parameterization was proposed by Pollard, Rhines & Thompson (1973), who assumed that entrainment was due mainly to shear instability of the Kelvin–Helmholtz type and therefore postulated a condition of marginal stability to describe averaged deepening. This technique has been used with some success by Price, Mooers & Van Leer (1978) in modelling observed oceanic deepening events. Kantha *et al.* report the occurrence of Kelvin–Helmholtz type behaviour in their experiments at least over a certain range

of overall Richardson number. Thorpe (1973*b*) has discussed observations of wave-like phenomena at turbulent interfaces and their possible role in entrainment.

Linden (1973) and Thompson (1974) have both attempted to model the mechanism of turbulent entrainment in the absence of mean shear. Linden's was an experimental study involving the interaction of a vortex ring with a sharp density interface. He measured the distortion of the interface due to the interaction and derived a simple argument leading to a power law relationship between entrainment rate and Richardson number. The argument used suggests that entrainment results as the buoyancy forces cause the interface to recoil, the ring to collapse and denser fluid to be ejected into the upper layer which then mixes with the fluid in the ring. The recoiling behaviour and subsequent mixing were observed on films of the experiment. Thompson solved numerically equations for the interaction of a vortex ring with a rigid wall. His solution may therefore only be valid for very large density differences. He attributes the motion of wisps of fluid away from the wall to the pressure field induced by the motion of the vortex ring. Fluid close to the wall is wrapped round the vortex rings and thus incorporated in the 'mixed layer'. A simple model of the wisp produces the same Ri relationship found by Linden and by Turner in his grid stirring experiments.

In density homogeneous flows the spread of a turbulent wake has been attributed to an average of a slow turbulent entrainment due to diffusion and amplification of vorticity and a faster entrainment mechanism due to an instability within the wake (see Townsend 1976). The different mechanisms have been clearly identified by a detailed study of the nature of the entrainment interface and of the structure of the turbulence and the mean flow at the interface and within the flow. Such detailed investigations have not yet been made for the stratified case. The presence of a density interface may modify the basic entrainment process not only by reducing the interfacial distortions and thus reducing the surface area over which the diffusive process can occur but also by superimposing one or other (or both) of the entrainment mechanisms postulated by Linden and Thompson.

In general both turbulent entrainment and Kelvin–Helmholtz instabilities will contribute to entrainment and the two processes may well be interdependent. Not only is the experience of entrainment investigations in density homogeneous flows useful in suggesting the kind of measurements that need to be made but also the many theoretical and experimental studies of instability in laminar flows that have been made (Drazin & Howard 1966; Hazel 1972; Thorpe 1971, 1973*a*; Patnaik, Sherman & Corcos 1976) will be useful in interpreting the observed instabilities in terms of other flow parameters.

This paper presents a description of the turbulent interface which is necessarily qualitative but which is a first attempt at trying to understand the relationship between the various interfacial phenomena observed in a turbulent density interface. It is hoped that in the near future a series of experiments can be carried out in which the required details of the flow field will be measured and that a clear picture of the nature of the entrainment process at density interfaces will emerge.

2. Notation

During the course of this paper a variety of quantities will be introduced and relationships between them will be sought. To avoid confusion all symbols used to denote these quantities will be defined now:

U_* friction velocity assumed to be the scale of turbulent velocity fluctuations
h mixed-layer depth
$\Delta\rho$ density difference across the interface
Ri_* Richardson number $= g\Delta\rho h/\rho_0 u_*^2$
δ_{int} distortion length scale due to eddies at the interface
a wave peak-to-trough amplitude
$a_{\max}$ maximum value of a
λ wavelength
S_l wave slope at maximum amplitude $= 2\pi a_{\max}/\lambda$
GR growth rate $= da/dt$
U_w phase speed of instabilities
U_i interface velocity scale
U_s screen velocity
δ length scale of velocity variation such that the difference in velocity through a distance δ is U_i
Ri interfacial Richardson number $= g\Delta\rho\delta/\rho_0 U_i^2$
V local velocity of advance of the entrainment interface
V_k Kolmogorov velocity scale
V_{ql} quasi-laminar entrainment rate
$\zeta(x,t)$ interface position ($\bar{\zeta} = h$).

3. Apparatus and data

The apparatus used by Kantha is described in detail in the report of the experiment (Kantha *et al.* 1977) and in Kato & Phillips' (1969) paper. A diagram of the apparatus is shown in figure 1. The tank has inner and outer diameters of 106·7 cm and 152·4 cm respectively. The channel cross-section is 22·8 cm wide and 28 cm deep. A surface stress was applied by rotating a plastic screen at the upper surface of the fluid in the tank. A two-layer stratified fluid system was produced with (initially) fresh water mixed with flourescin dye above a layer of salt solution. The interface was illuminated by a narrow slit of light through a glass window at the bottom of the tank so that about 8 cm along the interface (in the direction of rotation) could be seen. A second light was required to illuminate a centimetre scale which was used for calibrating the x, y co-ordinates of points on the interface. Kantha photographed the interface through a Plexiglas window in the side wall using a 16 mm movie camera. The interface is recorded on film as a layer of (usually) strong light intensity. Unfortunately the two light sources occasionally caused shadowing and this caused problems in measuring the interface position and shape from the films.

The films were projected onto a Hewlett-Packard digitiser so that the x, y co-ordinates of points of the interface could be recorded without too much difficulty. A stopwatch was mounted in the field of view of the camera and was used to determine

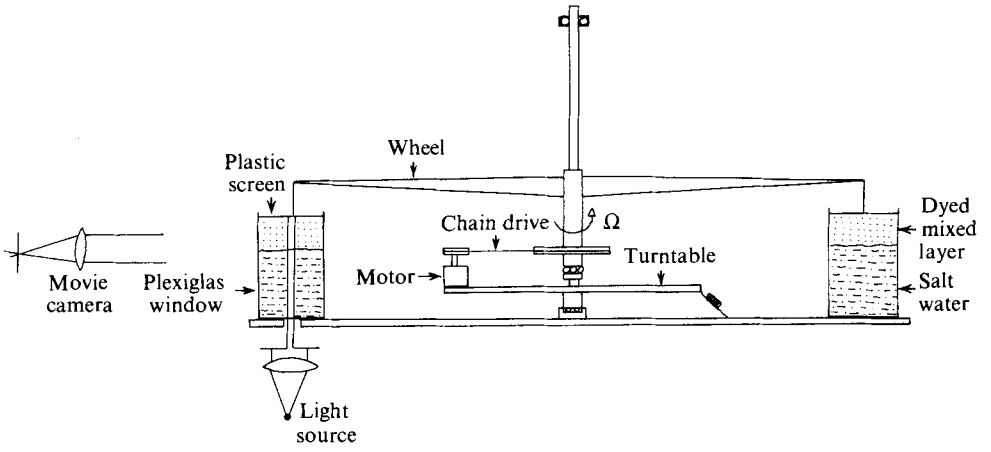

FIGURE 1. A sketch of the apparatus used by Kantha *et al.* (1977).

No. of runs	U_* (cm/s)	h_i (cm)	$\Delta\rho_i/\rho$	Ri_*
1	1·41	5·4	0·0135	36·0
1	1·41	5·4	0·0140	37·3
2	1·93	5·4	0·0235	34·0
1	1·41	5·4	0·0270	71·9
1	1·41	5·4	0·0275	73·2
2	1·93	5·4	0·0490	69·4
2	1·41	5·4	0·0550	146·4
2	1·93	5·4	0·0980	138·8

TABLE 1. Experimental parameter ranges. h_i, initial depth; $\Delta\rho_i$, initial density difference.

the time of an observation. Unfortunately the stopwatch and the centimetre scale were not always in focus simultaneously, so that reading the time from the watch was sometimes difficult. Any error in the time reading does not affect the relative times within the blocks of data defined below but would affect the time differences between blocks.

Kantha's experiments were conducted for a large range of Ri_* but because at large Ri_* it was possible to read the mixed-layer depth visually, films were made only for the low Ri_* experiments. The range of Ri_* and the other parameters that have been examined for details of the structure of the entrainment interface are shown in table 1. These Ri_* values can be contrasted with a value appropriate to typical oceanic conditions, e.g. with a 10 m s^{-1} wind, a mixed-layer depth of 20 m and a density difference of order 10^{-4}, $Ri_* = 126$.

Two sets of data were collected and will now be described.

3.1. *Turbulence data*

A typical data set is shown in figure 2(*a*). Each set consists of the x, y co-ordinates of 8 points along the interface separated in the x direction by about 1 cm. The data sets were measured every 2 or 3 frames of film. The data are divided into blocks which are made up of 10 data sets and which cover 2–4 s of the experiment. Deepening was not

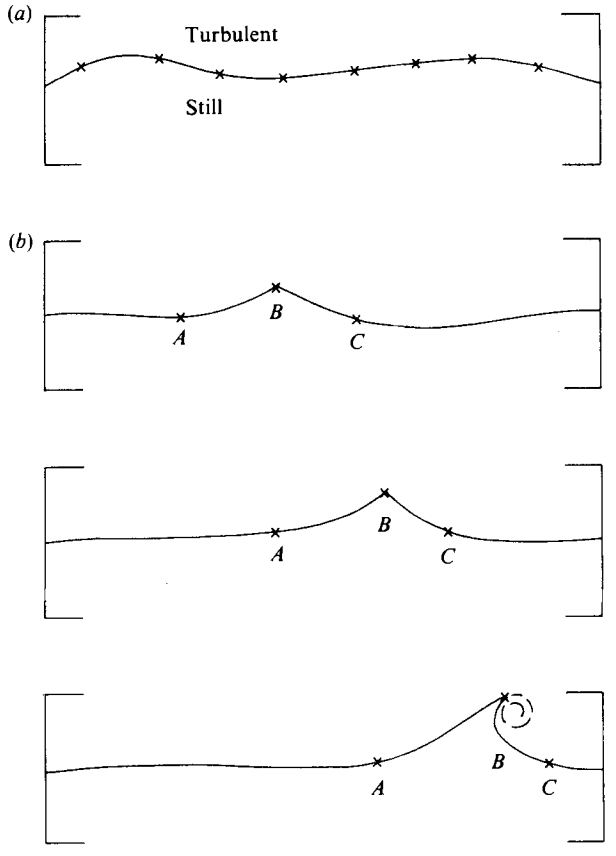

FIGURE 2. Schematic representation of (*a*) one frame of turbulence data; (*b*) three frames of wave data showing the development of an instability. ×, data point.

found to be significant during the period of one block. Blocks were collected at intervals of 5–10 s with occasional consecutive blocks during periods of wave-like activity. The number of blocks of data varied from film to film. For large Ri_* when the interface was fairly distinct 10–12 blocks of data were collected over a period of 80–160 s. For low Ri_* the interface was less distinct and the shadowing effect was more of a nuisance. Deepening was also more rapid and 5–6 blocks of data were collected over periods of 30–40 s. In all cases no measurements were made when the mixed-layer depth was greater than about 17 cm. At this depth the influence of the bottom boundary was beginning to be noticeable.

The accuracy of the z co-ordinate measurements varies with Ri_* with errors of ± 1 or 2 mm for large Ri_* increasing to ± 5 to 7 mm for low Ri_*. The errors are not constant for any one Ri_* and depend on the degree of shadowing and on the sharpness of the interface, which was seen to become more diffuse, and thus more difficult to measure, after the breakdown of an interfacial wave. Turbulence data are used to estimate the mixed-layer depth and a length scale associated with the shape of the interface. These will be discussed in § 4.

3.2. *Wave data*

A typical data series is shown in figure 2 (*b*). The film was run until the development of an instability was observed and was then reversed until the first indication of the

instability was seen. The co-ordinates of points A, B and C were measured frame by frame and describe the development of an instability from the time it is first observed until it either collapses or is advected out of the field of view. The lifetime of a wave is of order one second. The collapse of a wave in the form of a spiral was not always as clear as indicated in the diagram and was certainly not clear enough to be useful in estimating the amount of fluid entrained by such instabilities.

Because, in general, no more than one wave was visible at any one time, estimates of wavelength were difficult. A and C were usually chosen as points of minimum wave amplitude (maximum depth) and the difference in their x co-ordinates is used as an estimate of wavelength. B was chosen as the point of maximum wave amplitude and thus the difference between the z co-ordinate of B and the averaged z co-ordinates of A and C is an estimate of wave peak-to-trough amplitude.

The z co-ordinate measurements of wave data are generally more accurate than those of turbulence data since the onset and growth of an instability were often characterized by a sharpening of the interface. Although it was rare to observe more than one wave in one frame of film, the waves were generated in groups such that for a period of time waves would be generated, then none would be observed for about 10 s and then there would be another period of wave activity lasting from 1 to 5 s and occasionally as long as 10 s. Wave data are therefore divided into blocks of up to 10 wave histories (though usually less than 6). The number of blocks per film again varies with Ri_* with up to 9 blocks for Ri_* of order 140, up to 5 blocks for Ri_* of order 70 and for low Ri_*, order 35, no waves were clear enough to measure.

Apart from estimation of wavelength and amplitude, wave data are also used to determine growth rates and a velocity scale which will be used to construct an alternative Richardson number more appropriate to a description of the instability than Ri_*. The analysis of wave data is presented in §5.

4. Turbulence analysis

4.1. *The interface position*

A mean of all depths in one data block was calculated and identified with the mixed-layer depth h. This mean was determined to be accurate to within the assumed accuracy of measurement at the 95% confidence level. The standard deviation about this mean was used as an estimate of the distortion length scale δ_{int}. A necessary requirement is that deepening should be negligible within each data block. In all cases the change of depth during the period for which a block of data was being collected that would be predicted using Kantha's corrected deepening rates (which were corrected for side wall effects and were larger than the observed rates for given Ri_*) was less than δ_{int}. Estimates of δ_{int} in non-stratified flows show it to be related to the large flow scales, in this case h (see table 2) but with the ratio δ_{int}/h varying between flows. Gartshore (1966) has shown that δ_{int}/h is closely correlated with entrainment rate in non-stratified flows.

Figure 3 shows how the relationship between δ_{int} and h varies for different values of Ri_*. Least-squares fits to the data points are calculated and predict relationships of the form $\delta_{\text{int}} = ah + b$ where both a and b are found to vary with Ri_* (table 2). The statistical significance of these regressions (measured by looking at t-statistics of the regression coefficient and constant) decreases with increasing Ri_* until for Ri_* of

Ri_*	a	b	Correlation coefficient (δ_{int}, h)
140	0·00024	0·4	8×10^{-5}
70	0·031	0·18	0·3
35	0·067	−0·0051	0·6
Unstratified flows (Townsend 1976, table 6.2)			
$Ri_* = 0$			
Boundary layer	0·17	0	
Jet	0·22	0	
Wake	0·38	0	

TABLE 2. The variation with Ri_* of the regression constant b and regression coefficient a for the relation $\delta_{int} = ah + b$.

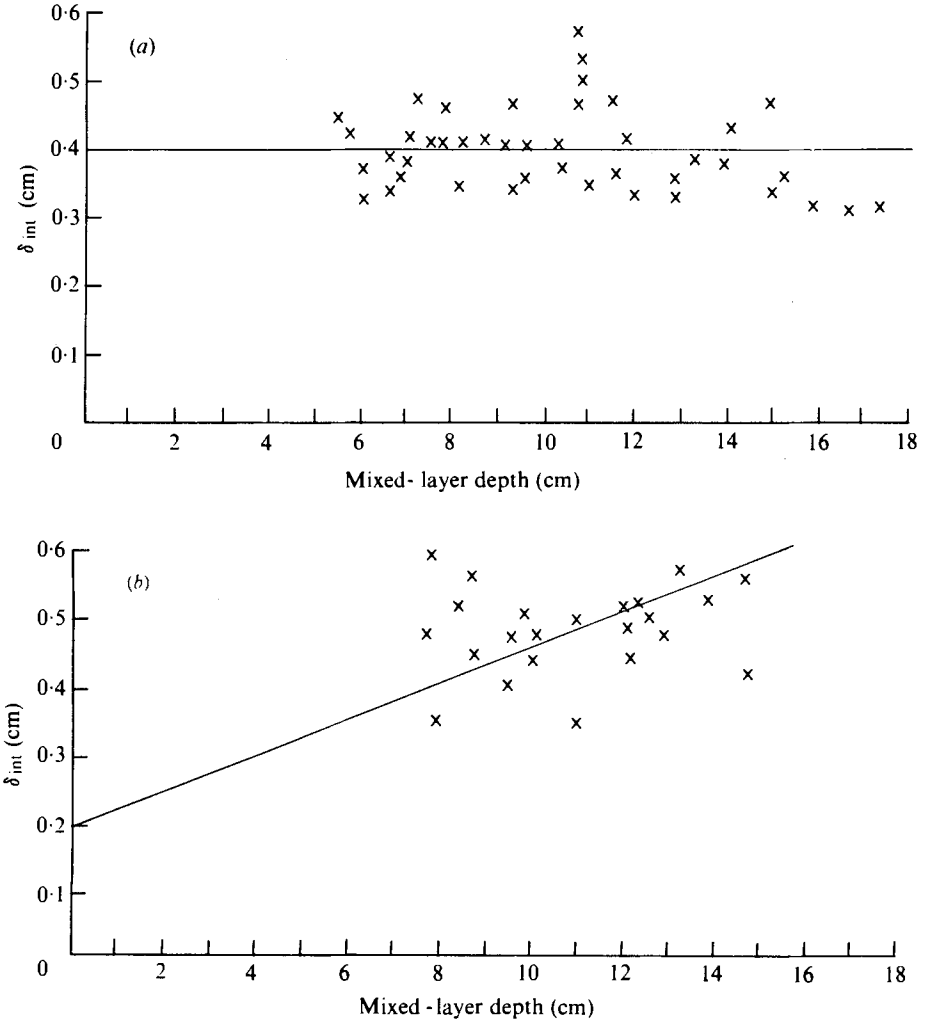

FIGURES 3(*a*, *b*). For legend see following page.

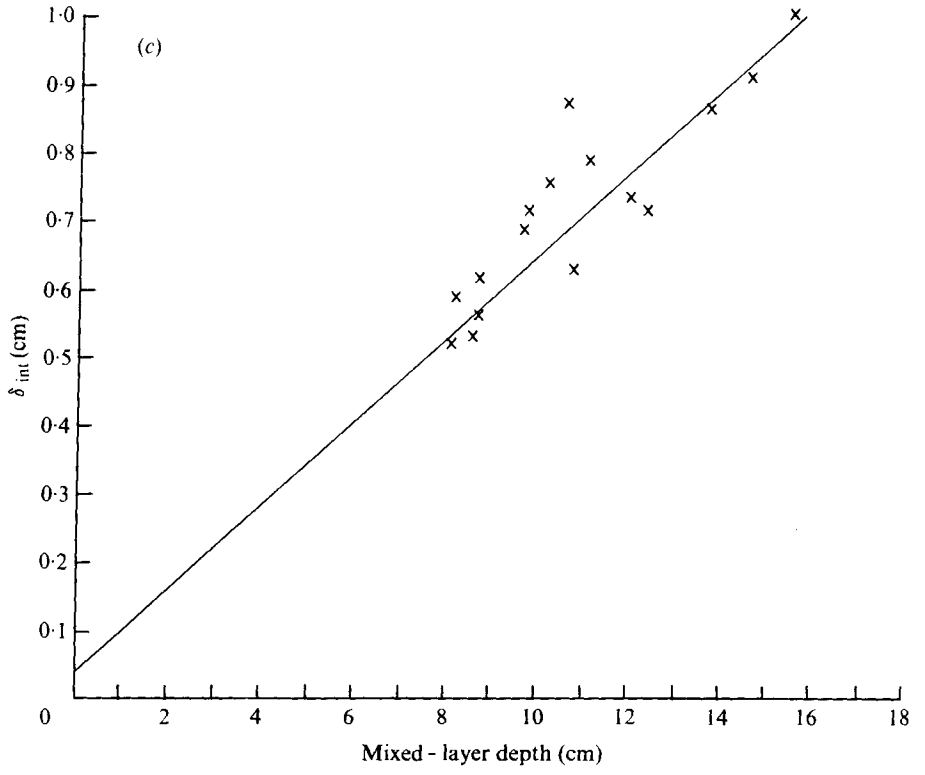

FIGURE 3. The dependence of distortion length scale δ_{int} on mixed-layer depth. ×, data point. Least-squares fits to the data points are shown. (*a*) $Ri_* \sim 140$; (*b*) $Ri_* \sim 70$; (*c*) $Ri_* \sim 35$.

order 140 there is very little correlation between δ_{int} and h. For Ri_* of order 70 a weak correlation is found which may suggest occasional dominance of the entrainment interface by large eddies with intermittent periods of small-scale eddy activity. Further discussion of the implications of these results is delayed until after details of the instability scales are presented. An explanation will then be offered for the large scatter of δ_{int} at large Ri_* (see § 6).

4.2. *The local velocity scale*

Phillips (1972) has related the entrainment rate in unstratified fluids to the shape of the entrainment interface in the following way:

$$U_e = V\overline{(1+(\nabla\zeta)^2)^{\frac{1}{2}}},$$

where V is the local velocity of advance of the entrainment interface perpendicular to itself, $\zeta(x,t)$ is the interface position. In unstratified fluids V has been assumed to be equal to V_k, the Kolmogorov scale. Phillips (1966) has suggested a second velocity scale, which will be referred to as V_{ql}, describing the quasi-laminar entrainment rate which is appropriate to the case when the turbulent front has length scale large compared with the scale of motion for which buoyancy forces become appreciable. In this case the interface is approximately horizontal so $U_e \sim V_{ql}$. The function $\overline{(1+(\nabla\zeta)^2)^{\frac{1}{2}}}$ will be called the shape factor in the discussion to follow.

Ri_*	Shape factor	U_e/U_* (Kantha)	V/U_*
140	1·056	0·047	0·045
70	1·104	0·0728	0·066
35	1·184	0·1098	0·093

TABLE 3. The variation with Ri_* of the local mean entrainment velocities related by $U_e = V \times$ shape factor.

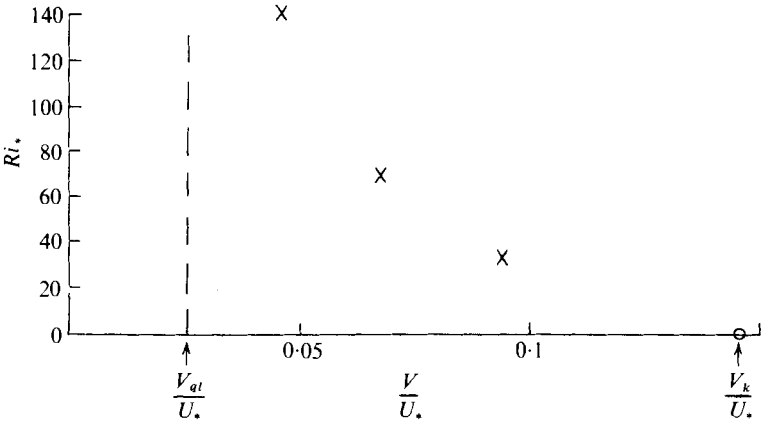

FIGURE 4. The variation of local entrainment velocity, V/U_*, with Ri_*. The quasi-laminar velocity scale V_{ql} and Kolmogorov velocity scale V_k are also shown.

$\nabla\zeta = \partial\zeta/\partial x$ (cross-stream variations have been assumed to be small) has been estimated from these data to determine the value of V in these flows. $\nabla\zeta$ is estimated as

$$\frac{\partial\zeta}{\partial x}(I) = \frac{z(I+1)-z(I)}{x(I+1)-x(I)}, \quad I = 1, \ldots, 7 \quad \text{(no. of data points in each set = 8)}.$$

Because the shape factor is found to be of order one (see table 3), the variation of V with Ri_* is very similar to the variation of entrainment rate U_e with Ri_*. For the purposes of these calculations Kantha's corrected entrainment rates will be used. Figure 4 shows the variation of V/U_* with Ri_*. Also shown are V_{ql}/U_* and V_k/U_* calculated as follows:

$$V_k = \left(\frac{U_*^3}{h}\right)^{\frac{1}{4}} \nu^{\frac{1}{4}},$$

$$V_{ql} = (\nu/h)^{\frac{1}{2}} U_*^{\frac{1}{2}} \quad \text{with} \quad \nu = 10^{-2}\,\text{cm}^2\,\text{s}^{-1},$$
$$h = 10\,\text{cm}.$$

The local dissipation rate has been estimated as U_*^3/h and U_* and h have been assumed to be the local turbulence scales. It is clear that if these estimates are correct (the results presented in §4.1 suggest that h at least may not be appropriate particularly in the estimate for V_{ql}; see also §6) the local advance of the interface is influenced by buoyancy but not to the extent of totally inhibiting the process of vorticity amplification due to the strain rates produced by small-scale eddies near the interface as is assumed in the derivation of V_{ql}.

5. Wave analysis

5.1. *Description of the instability*

There is a strong similarity between the development of instabilities at the interface in this experiment and those observed by Thorpe (1971, 1973*a*) at an interface in a laminar flow. The onset of instability is often characterized by a sharpening of the interface and a reduction in turbulent distortion of the interface. A small amplitude wave is seen which grows as it moves in the direction of the mean flow in the upper layer. It rolls up into a spiral, which soon collapses, and the interface becomes blurred. It is often possible to see the development of an instability from its inception to its final collapse, but sometimes, especially when long waves are generated, the wave is advected out of the field of vision before collapse has occurred.

Occasionally two waves appear simultaneously and after an initial period of growth one appears to absorb the other. This is a possible manifestation of a wave interaction described by Patnaik *et al.* (1976) and will be discussed below.

5.2. *Mean flow instability*

The similarity between the form of the instability observed here and that described by Thorpe for a laminar flow and calculated by Patnaik *et al.* suggests that it may be a mean flow instability. Mean flow instability can be characterized by an interfacial Richardson number based on the mean velocity variation and the density variation across the interface:

$$Ri = \frac{g\Delta\rho}{\rho}\frac{\delta}{(\overline{U_i})^2} \quad \text{where } \delta \text{ is a length scale associated with the mean velocity variation, } U_i.$$

Of these quantities, both δ and U_i are unknown in this case. ($\Delta\rho$ can be found using Ri_* and h.) If the velocity profile had been measured during the experiment then a comparison could have been made between observed and predicted wavelengths and growth rates to establish whether the instability is a simple mean flow instability or an instability of the total (i.e. mean + turbulent) flow. Although the velocity profile scales are not available it is possible to make some progress by using established relationships between certain wave and velocity profile scales. Theoretical studies of mean flow instability predict relationships between wavelength and interface thickness, phase speed and mean flow velocity. A Richardson number can therefore be constructed with the wavelength λ, and phase speed U_w, and can be compared with other parameters of the wave field. Its value can also be compared with the critical Richardson number (i.e. the minimum Richardson number for a stable interface) as a further check on the validity of the assumptions.

The velocity scale. The phase speed U_w of a wave at an interface can be shown to be equal to the mean speed of the flow, which in this case is $\frac{1}{2}U_i$ where U_i is the mean flow speed of the upper fluid at the interface and the lower fluid is assumed to be at rest. An estimate of U_w is obtained from the data by averaging the x co-ordinates of points A, B, C and calculating a least-squares fit to the variation of the average with time. Figure 5 shows a number of average position versus time plots. Standard statistical techniques (t-tests on the regression coefficient) were used to test the significance of

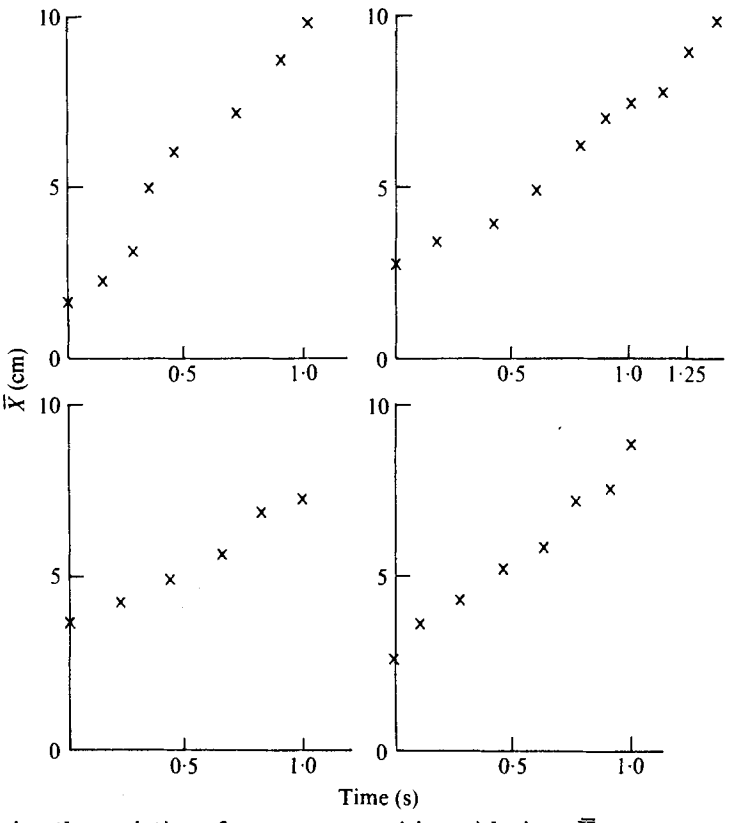

FIGURE 5. Showing the variation of mean wave position with time. $\bar{X}$, average x co-ordinate of points A, B, C in figure 2(b). Four examples taken from an $Ri_* \sim 140$ run.

the phase speed estimates. The phase speeds vary considerably from wave to wave (see figure 8). In one case the range was from 2·5 to 9·5 cm/s. It was first thought that these variations could be manifestations of the turbulent velocity field at the interface and that the shear generating the observed instabilities is due to the total velocity field not the mean flow. There are two main reasons why this hypothesis has been rejected. The velocity measurements are not accurate. Only three points on the wave were chosen to determine the average phase speed and one of these, point B, was observed to move with finite speed relative to A and C as wave growth occurred. Second, Richardson numbers based on calculated phase speeds do not show the influence on wave slope that was found by Thorpe (and is discussed below).

It was expected that the velocity at the interface, U_i, would be related to the screen velocity, U_s, which varied more smoothly with time and so a least-squares fit to the phase speed estimates, U_w, versus time was found and twice this was used to estimate U_i and hence Ri. U_w, U_i and U_s are compared in figures 6–8. (For clarity of presentation $\frac{1}{3}U_s$ is shown in the figures rather than U_s.) In most cases U_i was found to be related to U_s although there are not sufficient data to quantify this relationship and its variation with the other flow parameters. It must be emphasized that U_i is a very crude estimate of the mean interface velocity scale. Future investigation of the entrainment interface must include mean velocity measurements.

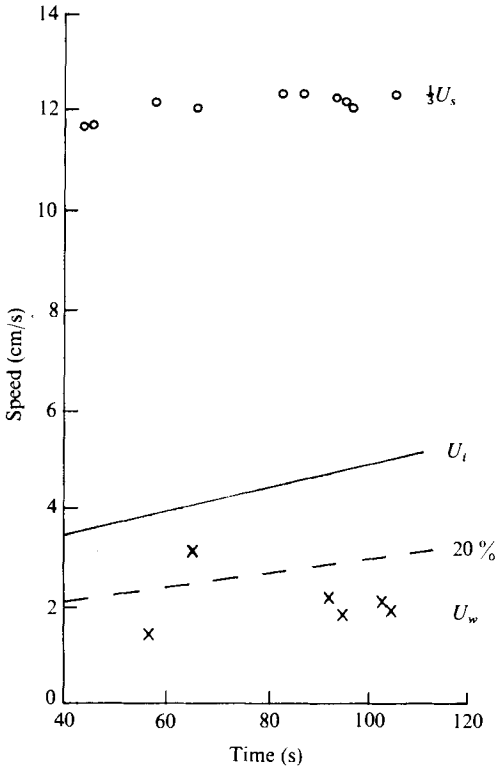

FIGURE 6. Mean flow velocity scales for $Ri_* \sim 70$, $U_* = 1{\cdot}93$. U_w, phase speed estimates; U_t, interface velocity scale; U_s, screen velocity measured by Kantha *et al.* (1977). ($\frac{1}{3}U_s$ shown for clarity of presentation.) Also shown is the 20 % increase in the least-squares fit to the U_w estimates.

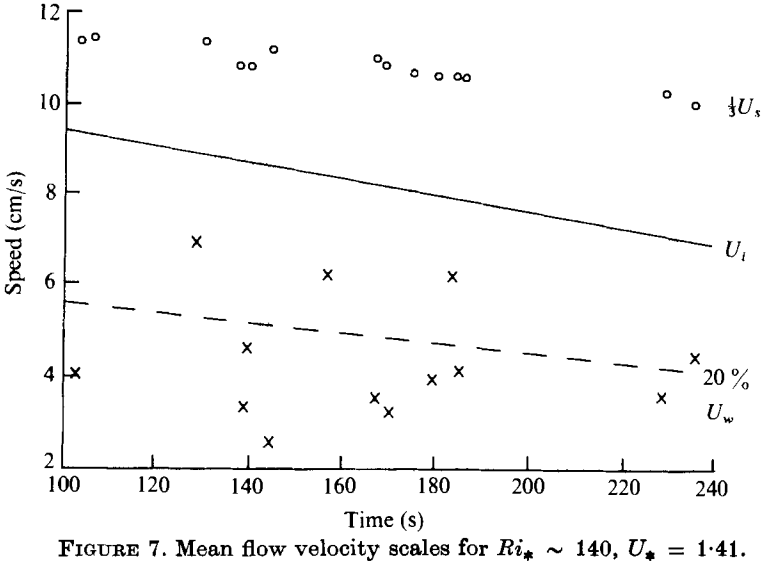

FIGURE 7. Mean flow velocity scales for $Ri_* \sim 140$, $U_* = 1{\cdot}41$. Notation as in figure 6.

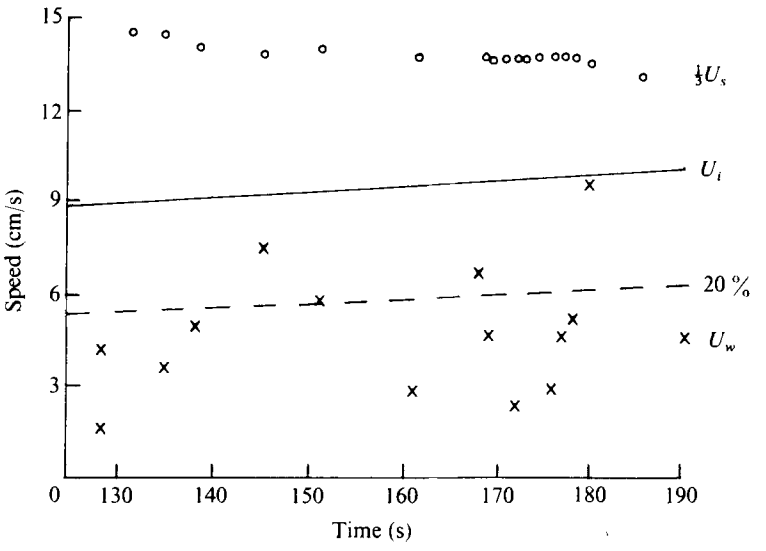

FIGURE 8. Mean flow velocity scales for $Ri_* \sim 140$, $U_* = 1{\cdot}93$. Notation as in figure 6.

The length scale. The wavelength, λ, of an instability is related to the width associated with the velocity shear at the interface, δ, by

$$\delta \times \frac{2\pi}{\lambda} \sim 0{\cdot}8.$$

This relationship varies slightly with Ri (see Hazel 1972) and Patnaik *et al.* have shown that nonlinear growth favours slightly longer waves, but for the purposes of this investigation it will be assumed to hold for all Ri.

No correlation is found between wavelength, λ, or maximum peak-to-trough amplitude, $a_{\max}$, and the mixed-layer depth, h. Thus the width of the shear layer, δ, is independent of the mixed-layer depth.

Richardson number. The values of Ri found using these velocity and length scales are usually less than 0·3,

$$Ri = \frac{g\Delta\rho}{\rho_0} \frac{(0{\cdot}8\lambda/2\pi)}{(U_i)^2}.$$

This is the order of magnitude of Richardson number required for instability to be possible.

The wave parameters that were used to make comparisons with laminar theory and experiment are the wave slope S_i (defined as $2\pi a_{\max}/\lambda$) and growth rate GR, non-dimensionalized with U_i. The variation of amplitude with time is used to estimate growth rates. Thorpe found for his experiments a variation in growth rate with time. In this experiment the amplitude estimates show erratic growth (see figure 9) and it seemed more appropriate to estimate an averaged growth rate for each instability. Least-squares estimates are obtained for each instability. These were tested using standard statistical techniques (90 % confidence limits were determined using the Student t-distribution) and the significant growth rate estimates are used in subsequent comparisons.

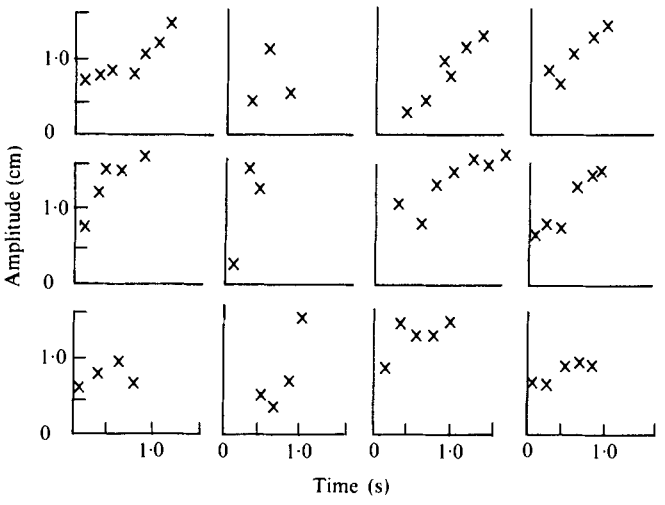

FIGURE 9. A series of amplitude/time plots for a $Ri_* \sim 140$ run, showing erratic growth.

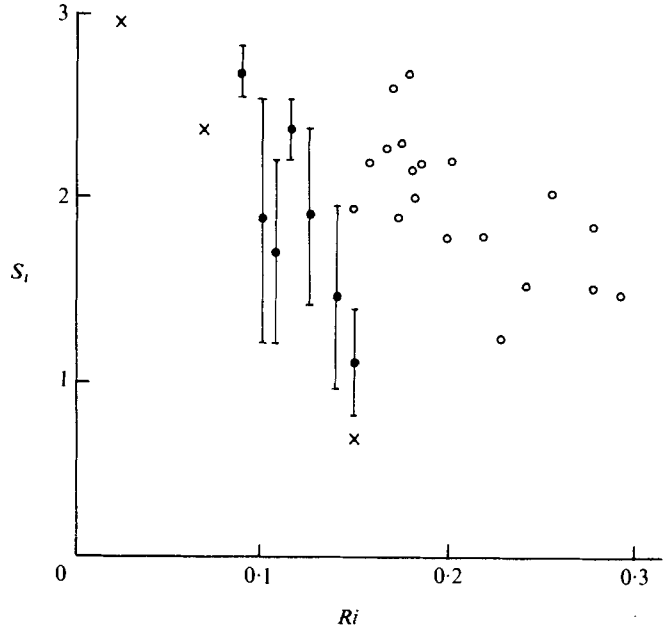

FIGURE 10. The variation of maximum slope S_l with Ri. ○, results of this investigation; ⧳, experimental observations from Thorpe (1973), mean and one standard deviation either side; ×, numerical results of Patnaik *et al.* (1976).

The S_l versus Ri comparisons are shown in figure 10. The decrease in S_l with increasing Ri is to be expected since U_i is only slowly varying and so Ri increases with λ. The measurements show a similar trend to both the Thorpe observations and the Patnaik *et al.* numerical predictions but the Richardson number range for fixed slope is shifted along the Ri axis. A 20% increase in U_i is required to bring the slope/Ri relationship calculated here into line with that found by Thorpe. Such an increase is

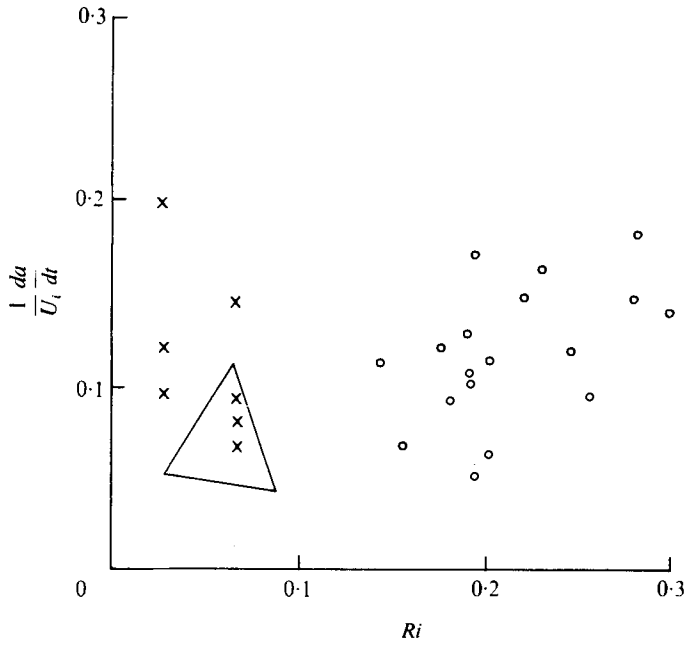

FIGURE 11. The variation of growth rate with *Ri*. Notation as in figure 10. Thorpe's results are scattered in the marked triangle.

within the range of phase speeds estimated from these data as can be seen in figures 6–8, where a 20 % increase in the least-squares fit to the U_w estimates is plotted.

A number of cases were found where the calculated wave slope was larger than expected for the calculated Richardson number. These generally fall into two categories. First there are those that seem to be examples of the rolling interaction described below. A Richardson number based on the wavelength of a subharmonic would be larger than the *Ri* at which the instability is generated. The remaining cases are based on measurements of isolated instabilities (i.e. only one wave in a block) with wavelengths larger than the average for the experiment which could also have been generated by a wave interaction occurring outside the field of view.

The non-dimensionalized growth rates show large scatter and as can be seen in figure 11 do not compare well with Thorpe's observations or Patnaik *et al.*'s predictions. Once again a 20 % increase in the velocity scale brings the results more into line with those of Thorpe since this would not only reduce *Ri* but would also reduce the non-dimensional growth rates. Thorpe's results indicate an increase in growth rate with *Ri* contrary to the numerical predictions. This trend is also seen in these observations. The comparison between instabilities generated at a turbulent/laminar interface and those observed by Thorpe in the non-turbulent case is only valid if instabilities develop independently of the turbulence. Any transfer of energy between the developing instabilities and the turbulence will lead to maximum wave slopes and growth rates which differ from those observed in non-turbulent flows. The differences between these results and those of Thorpe and Patnaik *et al.* could be interpreted as a transfer of energy to the instability from the turbulence thus causing the instability to be more energetic for given wavenumber than would be the case in a non-turbulent flow. This

is the reverse of what would be predicted if the effect of turbulence is modelled by an eddy viscosity as has been assumed in the stability analyses of Townsend (1966) and Reynolds (1972) for density homogeneous flows. However eddy viscosity models are only appropriate if the length and velocity scales associated with the instability are large compared with those of the turbulence. This is probably not the case here and so a different interaction between instability and turbulence is possible.

Resonant interactions. Numerical experiments of Patnaik *et al.* simulate interactions between a wave of wavelength given by linear prediction of the fastest growing wave and its first subharmonic. Two different types of interactions are predicted. When the subharmonic is in phase with the primary wave, the subharmonic grows at the expense of the primary wave. This has been termed a rolling interaction because it manifests itself as two consecutive peaks rotating about their common trough. Examples of this were observed. When there is a phase difference of π the primary wave is annihilated with very little obvious development of the subharmonic. Observations were made of cases when two waves of similar wavelength were present simultaneously in the field of view but which did not seem to develop into the characteristic spiral form. These may be examples of a shredding interaction.

The possible development of either interaction is important because it does imply that a simple Ri criterion may not be sufficient to describe the entrainment due to mean flow instability. The rolling interaction will produce a larger contribution to entrainment than would have been predicted and the second interaction would produce none at all.

6. The interaction of turbulence and instability

Neither the distortion length scale nor the wavelength of the instability were found to be related to h. There does appear to be a relationship between these two length scales. Figure 12 is a plot of δ_{int} versus λ. The δ_{int} values are representative of the turbulent interface at the time the wave was being measured but because they are averaged over a longer time than a wave lifetime they are more representative of the general turbulent field than estimates of the averaged wave amplitude. A relationship is found with λ increasing as δ_{int} decreases. A dependence on U_* is also seen with λ decreasing for fixed δ_{int} as U_* increases.

Intuitively one would expect the distortion at the interface to be related to the scale of energy containing eddies near the interface. Not only is this found to be true in density homogeneous flows but the investigation of Linden (1973) suggests that it should also be true for two-layer flows. The results of § 4.1 imply that as Ri_* increases there are times when the energy containing eddies at the interface do not scale with the mixed-layer depth and for $Ri_* \sim 140$ this situation seems to occur throughout the experiment.

In this experiment the two main sources of turbulent energy at the interface are the flux from the mixing layer and local shear production. If the dominant source is shear production the energetic eddies will scale with the length scale associated with the shear. In this case a direct relationship is expected between the eddy length scale and the instability length scale. The results shown in figure 12 suggest that the length scale of the shear layer is intermittent. A decrease in length scale will result in smaller instabilities but, if the velocity difference is approximately constant, there

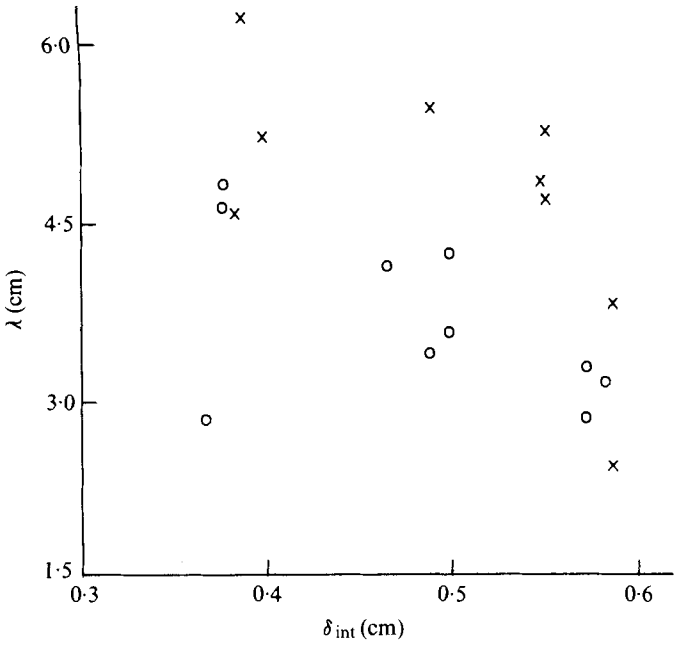

FIGURE 12. The relationship between distortion length scale δ_{int} and wavelength showing the variation with friction velocity, U_*. ×, $U_* = 1{\cdot}41$; ○, $U_* = 1{\cdot}93$.

will be an increase in shear production and the eddies may be more energetic resulting in an increase in distortion scale. An intermittency in the shear scale can also explain the small correlation between δ_{int} and h at $Ri_* \sim 70$. When shear production is large energetic eddies will scale with the local length scale, when it is small the flux term may dominate and the mixed-layer depth will be the appropriate scale.

A region of large shear at the turbulent/non-turbulent interface is not observed in a density homogeneous flow. The reason why it should develop when there is a density interface is beyond the scope of this investigation. However it appears that if the shear is sufficiently strong (as measured by a local gradient Richardson number) the region is self-maintaining.

A quantitative analysis of the various time and length scales that describe the relative importance of the two sources of turbulent energy and their roles in entrainment awaits a detailed examination of the mean and turbulent velocity and density fields throughout the mixed layer and interface.

7. Summary

The work presented in this paper provides a qualitative description of the nature of the turbulent interface in a two-layer flow.

Details of the instabilities generated at the interface have been measured and appear to be mean flow instabilities of the Kelvin–Helmholtz type with properties similar to those observed in non-turbulent shear flows.

It has been demonstrated that the length scale of interfacial distortions does not always scale with the mixed-layer depth, a feature particularly apparent at the larger

values of the overall Richardson number, Ri_*, for which measurements were made. This has been interpreted as a manifestation of a distinct region of small-scale eddies near the interface maintained by local shear production. The existence of a region of shear with length scale independent of the mixed-layer depth has been inferred from measurements of Kelvin–Helmholtz instabilities at the interface. The mechanisms that lead to the development of such a region cannot be determined with these data but are the subject of current research.

It is clear that the amount and quality of the data presented here are not sufficient to allow a complete description of the entrainment mechanisms. The investigation demonstrates the need for a detailed quantitative study of the mean and turbulent velocity and density fields throughout the flow.

This research has been supported by the Natural Environment Research Council and by Office of Naval Research Contract N0014-75-C-0700. The work is based on the author's Ph.D. thesis (University of Southampton, 1976). The advice and guidance of R. T. Pollard is gratefully acknowledged. Special thanks are expressed to O. M. Phillips and L. H. Kantha for providing the films and for many valuable discussions.

REFERENCES

DENMAN, K. L. 1973 A time-dependent model of the upper ocean. *J. Phys. Ocean.* **3**, 173–184.

DRAZIN, P. G. & HOWARD, L. N. 1966 Hydrodynamic stability of parallel flows of inviscid fluid. *Adv. Appl. Mech.* **9**, 1–89.

GARTSHORE, I. S. 1966 An experimental examination of the large-eddy equilibrium hypothesis. *J. Fluid Mech.* **24**, 89–98.

HAZEL, P. 1972 Numerical studies of the stability of inviscid stratified shear flows. *J. Fluid Mech.* **51**, 39–61.

KANTHA, L. H., PHILLIPS, O. M. & AZAD, R. S. 1977 On turbulent entrainment at a stable density interface. *J. Fluid Mech.* **79**, 753–768.

KATO, H. & PHILLIPS, O. M. 1969 On the penetration of a turbulent layer into a stratified fluid. *J. Fluid Mech.* **31**, 643–655.

KRAUS, E. B. & TURNER, J. S. 1967 A one-dimensional model of the seasonal thermocline: II. The general theory and consequences. *Tellus* **19**, 98–106.

LINDEN, P. F. 1973 The interaction of a vortex ring with a sharp density interface: a model for turbulent entrainment. *J. Fluid Mech.* **60**, 467–480.

MOORE, M. J. & LONG, R. R. 1971 An experimental investigation of turbulent stratified shearing flow. *J. Fluid Mech.* **49**, 635–655.

PATNAIK, P. C., SHERMAN, F. S. & CORCOS, G. M. 1976 A numerical simulation of Kelvin–Helmholtz waves of finite amplitude. *J. Fluid Mech.* **73**, 215–240.

PHILLIPS, O. M. 1966 *The Dynamics of the Upper Ocean.* Cambridge University Press.

PHILLIPS, O. M. 1972 The entrainment interface. *J. Fluid Mech.* **51**, 97–118.

POLLARD, R. T., RHINES, P. B. & THOMPSON, R. O. R. Y. 1973 The deepening of the wind-mixed layer. *Geophys. Fluid Dyn.* **4**, 381–404.

PRICE, J. F., MOOERS, C. N. K. & VAN LEER, J. C. 1978 Observation and simulation of storm-induced mixed-layer deepening. *J. Phys. Ocean.* (to appear).

REYNOLDS, W. C. 1972 Large-scale instabilities of turbulent wakes. *J. Fluid Mech.* **54**, 481–488.

THOMPSON, S. M. 1974 Interaction of a vortex ring with a rigid plane: a model for turbulent entrainment. *New Zealand Ministry of Works Rep.*

THORPE, S. A. 1971 Experiments on the instability of stratified shear flows: miscible fluids. *J. Fluid Mech.* **46**, 299–319.

THORPE, S. A. 1973*a* Experiments on instability and turbulence in a stratified shear flow. *J. Fluid Mech.* **61**, 731–751.

THORPE, S. A. 1973*b* Turbulence in stably stratified fluids: a review of laboratory experiments. *Boundary-Layer Met.* **5**, 95–119.

TOWNSEND, A. A. 1966 The mechanism of entrainment in free turbulent flows. *J. Fluid Mech.* **68**, 297–308.

TOWNSEND, A. A. 1976 *The Structure of Turbulent Shear Flow.* Cambridge University Press.

TURNER, J. S. 1968 The influence of molecular diffusivity on turbulent entrainment across a density interface. *J. Fluid Mech.* **33**, 639–656.

TURNER, J. S. 1969 A note on wind mixing at the seasonal thermocline. *Deep-Sea Res. Suppl.* **16**, 297–300.

WYATT, L. R. 1976 Mixing and stratifying processes in the oceanic surface layer and seasonal thermocline. Ph.D. thesis, University of Southampton.